



Preparation of acylated microcrystalline cellulose using olive oil and its reinforcing effect on poly(lactic acid) films for packaging application

Ravindra D. Kale¹ · Vikrant G. Gorade¹

Received: 9 November 2017 / Accepted: 29 January 2018 / Published online: 16 February 2018
© Springer Science+Business Media B.V., part of Springer Nature 2018

Abstract

A novel poly(lactic acid) (PLA) based composite, reinforced by microcrystalline cellulose (MCC) was prepared. MCC was modified by esterification reaction using olive oil for improving the compatibility with PLA matrix. The acylated microcrystalline cellulose (AMCC) exhibited reduced polarity in comparison to unmodified MCC. AMCC/ PLA composite films were prepared using solvent casting technique. The effects of the MCC surface modification on morphological, mechanical, physical, thermal, biodegradability and barrier properties of the PLA based MCC composites were studied. FTIR analysis confirmed acylation reaction of MCC. Scanning electron microscopy analysis exhibited a uniform distribution of AMCC in PLA matrix. Barrier properties of AMCC based composites were improved as compared to MCC based composites. The tensile strength and tensile modulus of composite films (at 2 wt.% AMCC) were improved about 13% and 35% as much as those of the pure PLA films, respectively. These biodegradable composite films can be a sustainable utilization of olive oil and microcrystalline cellulose in the food packaging application.

Keywords Bioresource · Microcrystalline cellulose · Olive oil · Surface acylation · Ultraviolet protection · Biodegradability

Introduction

Microcrystalline cellulose (MCC) is a ubiquitous and abundant structural polymer found in various plant sources. Commercially it is available as a partially purified, depolymerized α -cellulose. MCC has the benefit of its morphology, low density, mechanical strength [1, 2], high crystalline content and high specific surface area compared to other conventional cellulose fibres. Therefore, it is a very promising natural polymer as a reinforcing material in the polymer matrix. Recently, improvements in the functional properties of packaging films have been made by reinforcement of the polymer matrix with layered silicates [3]. Many researchers have modified the MCC with inorganic materials to improve several properties such as thermal conductivity and

mechanical strength [4]. It has also been used in many industries like cosmetics, plastics, food, and pharmaceuticals, due to its excellent properties [5].

MCC have been used as a reinforcing material in a wide range of synthetic polymer matrix [6–12], such as poly(methylmethacrylate) [13], poly(caprolactone), polyurethane [14], and poly(lactic acid) [15–17] etc. PLA is widely used to prepare biodegradable packaging films because of its biodegradability, high transparency, clear printability and excellent processability. PLA is being used as commercial food packaging products having a short shelf life in a typical application such as drinking cup, lamination films, carry bag, overwrap, containers etc. [18].

Weak interaction between PLA and MCC is a major limitation to get superior properties of composite films. This weak interaction is because of availability of hydroxyl group of MCC which is responsible for moisture absorption causes weak interfacial bonding between MCC and PLA. This limitation can be overcome by chemical modification of MCC using various chemicals like stearic acid, isocyanates [19], fatty acid derivate [20], benzylation [19], silane [21], permanganate [22], sodium chloride and fungal [23], grafting of

✉ Ravindra D. Kale
rd.kale@ictmumbai.edu.in

✉ Vikrant G. Gorade
vikrantgorade29@gmail.com

¹ Department of Fibres and Textile Processing Technology, Institute of Chemical Technology, Nathalal Parekh Marg, Mumbai, Maharashtra 400019, India

methyl acrylate, styrene [24], acetic anhydride [25], maleated coupling agents [26], alkenyl succinic anhydride [27], and peroxide [28] etc.

Modification of MCC using these chemicals is not a sustainable process, additionally they have restrictions regarding volatility, toxicity and instability in reaction processing, to overcome this problem ecofriendly reacting agents from natural sources can be a possible solution [29]. Olive oil has potential in green chemistry and bio-based approach to accomplish water repellency on natural hydrophilic polymers like cellulosic materials. It is abundant, readily available, cheap, and replenishable bioresource mainly used in food applications.

In this study, the surface of MCC was acylated using olive oil to improve the dispersion of MCC in the PLA matrix. To best of our knowledge, this reaction has not been exploited for the modification of MCC and not been applied in PLA-based composites. The composite films were prepared with the AMCC and MCC, as a reinforcing material in PLA matrix using solution casting technique. FTIR study confirmed acylation of MCC. The behaviour of MCC and AMCC dispersion in PLA matrix on physical, mechanical, thermal, barrier and biodegradability properties are investigated.

Experimental

Materials

PLA (PLA 6201D) with a specific gravity of 1.24 g/cm³ was provided by Nature Works®, USA. MCC (Arbocel UFC 100, white powder, particle size in the range of 13–15 µm) was procured from J. Rettermaier India Pvt. Ltd., Mumbai, India. Olive oil used was procured from SK Oil Industries, Mumbai, India. Ethanol and chloroform (AR grade) were bought from SD Fine Chemical Ltd., India.

Modification of MCC

MCC was modified using olive oil as described by *Dankovich et al.* [30], with minor modification in their method. MCC suspension of 6% (w/w) was prepared in distilled water and was subjected to high-speed homogenizer (IKA T25, digital Ultra Turrax, IKA® India Pvt. Ltd., Karnataka, India) at 6500 rpm for 1 h. The suspension was then centrifuged using centrifuge machine (R-8C, Rami, Mumbai, India) at 2500 rpm for 15 min. The resultant solid residue was dried at 65 °C in hot air oven (MSI-5, Meta-lab Scientific Industry, Mumbai, India) for 6 h. This ultrafine MCC was used for modification.

2 ml of olive oil was dispersed in 60 ml of ethanol (1:30, v/v) in sonicator with 20 mm probe (PR-1000MP, Ultrasonic Processor Sonapros, Mumbai, India) for 5 min with 600 W power. 5 g of ultrafine MCC was added to this homogenous

mixture and again sonicated for 5 min. The sample was air dried at room temperature to evaporate ethanol. For esterification reaction, the samples were kept in a hot air oven at 110 °C for 30, 60 and 90 min. Excess of un reacted olive oil was removed by immersion in ethanol for 15 min three times at room temperature, each time using fresh solvent. The modified ultrafine MCC was dried in hot air oven at 65 °C for 60 min and called as AMCC. Higher acyl % of AMCC was used for the preparation of composite film.

PLA composite film preparation

Biodegradable PLA/AMCC composite film was prepared by solution casting method. For casting of the composite film, 5 wt.% stock solutions of PLA were prepared by dissolving PLA chips in chloroform solvent at room temperature. The solution was continuously stirred until the PLA chips were completely dissolved. Blank film of PLA (without any MCC or AMCC), PLA/MCC (0.1, 0.5, 1 and 2 wt.%) and PLA/AMCC (0.1, 0.5, 1 and 2 wt.%) were obtained by using 50 ml of PLA solution. The mixtures were then poured into A4 size glass mould and kept in a vacuum dryer to evaporate chloroform at ambient temperature for 6 h. The composite films were kept in a hot air oven at 40 °C for 60 min for drying.

Characterization

Estimation of acyl group content

The percent acylation of AMCC sample was calculated by using titration method. 4 g AMCC was taken in 250 ml conical flask having 50 ml of ethanol:water solution in 3:1 ratio at 50 °C for 30 min with constant stirring. The solution was maintained at room temperature for cooling after which 40 ml of 0.5 M KOH solution was added to it. The excess of alkali was titrated against 0.5 M HCl using phenolphthalein as an indicator. Titration was carried out until the colour transformed from pink to colourless. Blank reading was taken using MCC sample [31]. The percent acylation of AMCC sample was calculated using Eq. (1):

$$Acyl\% = \frac{\{(V_B - V_S) \times M\} + \{0.043 \times 100\}}{W} \quad (1)$$

Where,

V_B Volume (ml) of 0.5 M HCl required for titration of the blank,

V_S Volume (ml) of 0.5 M HCl required to titrate the sample,

M Molarity of used HCl,

43.05 g·mol⁻¹ Molecular weight of the acetyl group,

W Dry weight of the sample (g).

Wettability test by nonpolar solvent

Wettability of MCC and AMCC was evaluated using 0.5 g sample by visual assessment using 20 ml water/toluene solvent system in 1:1 ratio, which has different polarities and densities [32].

Fourier transform infrared (FTIR) spectroscopy

The MCC and AMCC samples were prepared by pelletizing them with KBr (1:100 w/w), and FTIR was recorded on FTIR-8400S spectrometer (Shimadzu Corporation, Japan) at 4.0 cm⁻¹ resolution from 650 to 4000 cm⁻¹ and 32 scans per sample.

Thickness measurements

The thickness of the PLA (Blank), PLA/MCC and PLA/AMCC samples were measured using Digital Vernier Caliper of Mitutoyo Corporation, Japan. Total 40 measurements were taken at different places for each sample and average was reported.

Moisture absorption test

The composite films were cut in the dimension of 2 cm × 2 cm, initial weight of this sample was noted. All composite films were immersed in water for 24 h at room temperature. All samples then take out and allow to air dry for 1 h. The weight was taken as a final weight. The procedure was repeated 5 times, and average weight was taken for the further calculation. The % weight gain at equilibrium because of moisture absorption (Me) was determined using Eq. (2) [33]:

$$Me = \frac{W_f - W_i}{W_i} \times 100 \quad (2)$$

Where,

W_i Initial dry weight (g) and

W_f Final weight of composite film (g).

Water vapour permeability (WVP) tests

WVP tests of PLA (Blank), PLA/MCC and PLA/AMCC composite films were carried out according to ASTM E96–2005 test method B [34, 35].

Morphological study

The surface morphology of the broken composite films was analyzed using SEM, XL 30 (Philips, The Netherlands).

Before scanning, all samples were coated with gold for 3 to 4 min using sputter coater to dissipate the static charges generated due to electron bombardment with accelerated electrons having 12 kV energy.

X-ray diffraction (XRD) analysis

XRD patterns were obtained using X-ray diffractometer, XRD-6100 (Shimadzu, Japan) at 40 kV and 30 mA using Cu-K α radiation. The angular range (2 θ) was taken from 5 to 45° and using continuous mode of scanning, the measurement was made with the sampling pitch of 0.02°, at the rate of 2°/min.

Mechanical properties

Mechanical testing of PLA (Blank), PLA/MCC and PLA/AMCC were performed on Tinius Olsen Inc., Model H5KS (Horsham, PA, USA) testing machine with a load cell of 10 kN and a crosshead speed of 2 mm/min. Tensile strength was measured as per ISO 527 standard. Testings were repeated five times, and the results are presented as average for tested samples.

Thermal properties

The thermal stability and decomposition study of PLA (Blank), PLA/MCC and PLA/AMCC composite films was done on the thermogravimetric analyzer, TG-60H (Shimadzu, Japan). All composite films were analysed under nitrogen atmosphere of 100 ml/min flow rate with a heating rate of 10 °C/min in the temperature range of 25 °C to 500 °C.

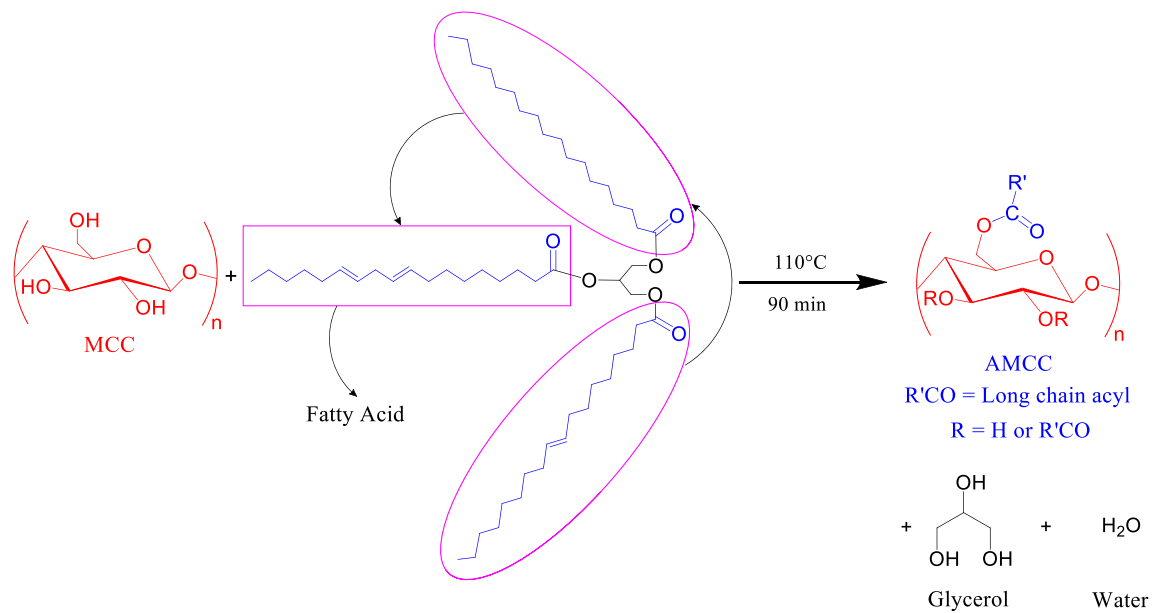
UV-protection of PLA composite film

The ability of composite films to block UV light is given by the ultraviolet protection factor (UPF) values. The UPF values were calculated according to AS/NZ 4399 standard. Measurements were performed in a UV spectrophotometer UV-2600 (Shimadzu, Japan) using an integrating sphere load in the region of 290 nm to 400 nm at an interval of 5 nm. The percentage blockings of UV-A (315–400 nm) and UV-B (280–315 nm) were calculated from the transmittance data [36]. UVA, UVB and UPF values were calculated using the following equations:

$$UVA = \frac{T_{315} + T_{320} + T_{325} + \dots + T_{395} + T_{400}}{18} \quad (3)$$

$$UVB = \frac{T_{290} + T_{295} + T_{300} + T_{305} + T_{310} + T_{315}}{6} \quad (4)$$

$$UPF = \frac{\sum_{\lambda=290}^{400} E_{\lambda} \times E_{\lambda} \times \Delta\lambda}{\sum_{\lambda=290}^{400} E_{\lambda} \times E_{\lambda} \times T_{\lambda} \times \Delta\lambda} \quad (5)$$



Scheme 1 Transesterification reaction between MCC and olive oil

Where,

- E_λ Erythematous spectral coefficient for each wavelength
 S_λ Solar spectral irradiance for each wavelength
 T and T_λ Transmittance at each wavelength
 $\Delta\lambda$ Measurement wavelength interval (nm).

The UPF equation weighs the UV-B radiation more heavily than UV-A.

Biodegradability of PLA composite film

The PLA (Blank) and PLA composite films were cut in the size of 30 mm x 30 mm. The test was carried out on a rectangular tray (20 cm × 15 cm) containing garden soil

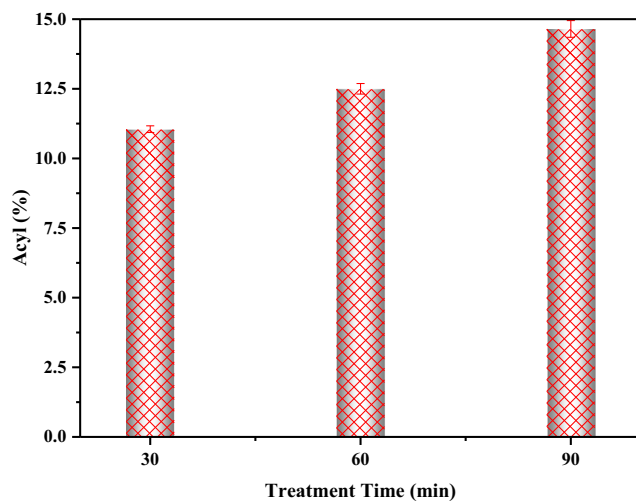


Fig. 1 Acyl % of AMCC samples with increasing reaction treatment time between MCC and olive oil

having 95% humidity by daily spraying it with water. All composite films were buried in this soil at room temperature for 90 days. Each sample was taken out of the soil at a specific time interval, washed with water and dried at 55 °C for 24 h, take out in decigator for 60 min and weighed. % weight loss of each sample was calculated by using the initial and final weight of the sample.

Result and discussion

Acylation of MCC

The acylation of MCC by olive oil is shown in Scheme 1. Long chain acyl group of olive oil gets

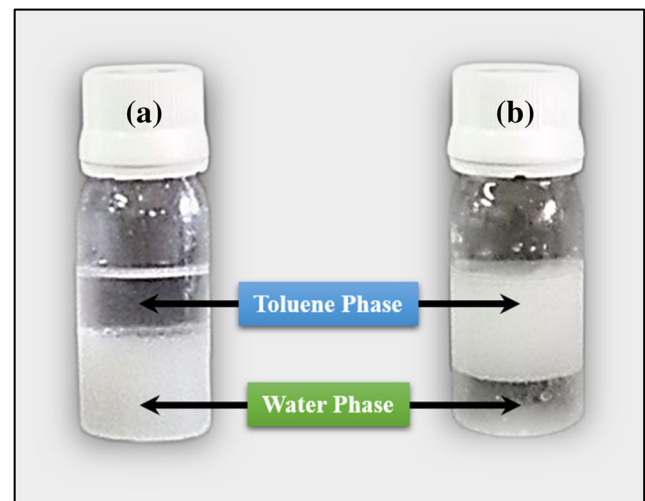
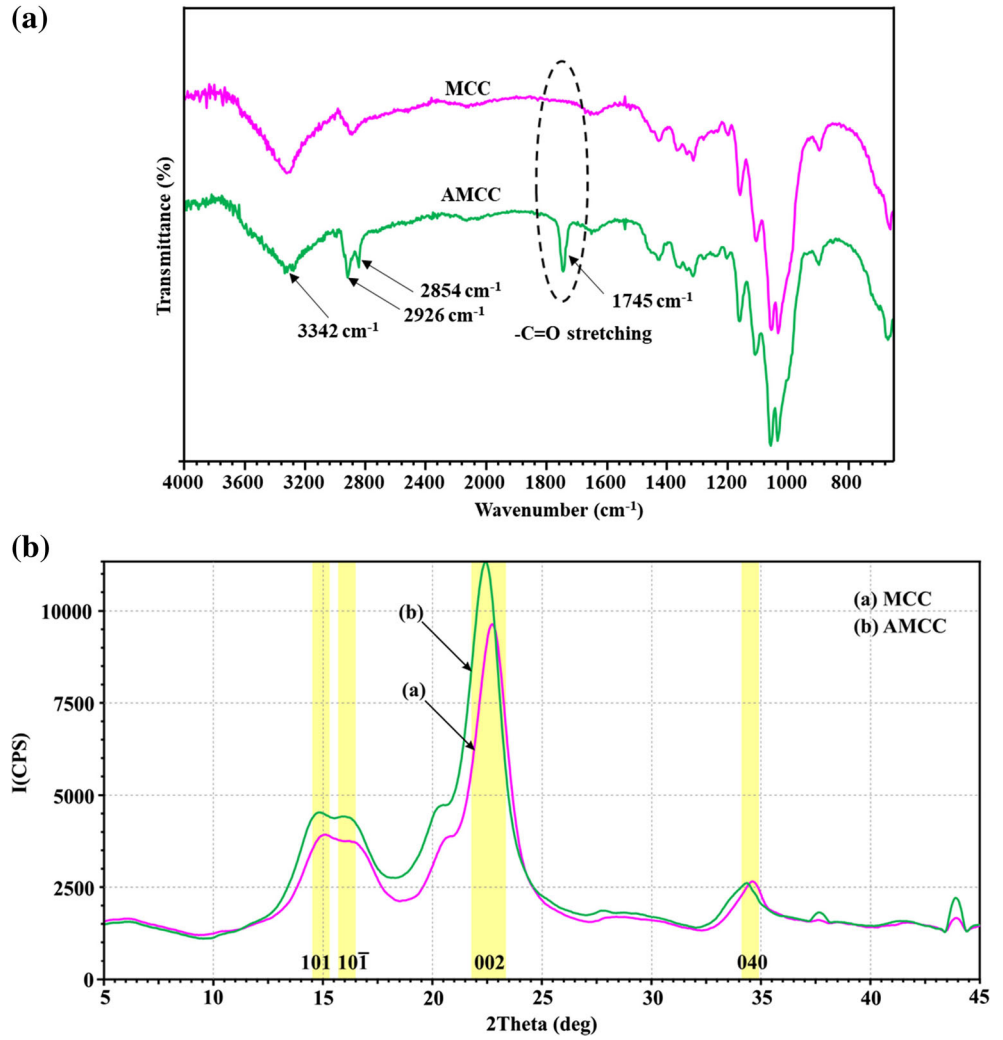


Fig. 2 Dispersion images of the MCC (a) and AMCC (b) suspended in a water-toluene solvent system

Fig. 3 FTIR spectra (a) and X-ray diffraction patterns (b) of MCC and AMCC with 2 ml olive oil at 110 °C for 90 min



covalently bonded to the hydroxyl group of MCC [30]. Figure 1 shows the % acylation of MCC with increasing treatment time at 110 °C. It was observed that %

acylation of MCC increased with increasing treatment time. AMCC modified for 90 min was used for the preparation of composite films.

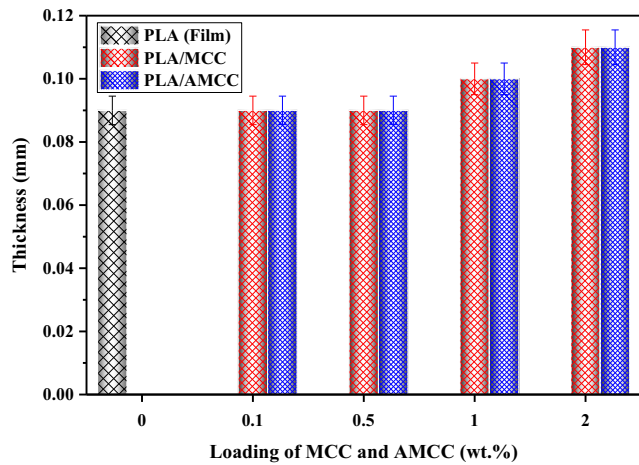


Fig. 4 Thickness of PLA (Blank), PLA/MCC and PLA/AMCC (different loading 0.1, 0.5, 1, 2 wt.% loading of MCC and AMCC respectively) of composite films

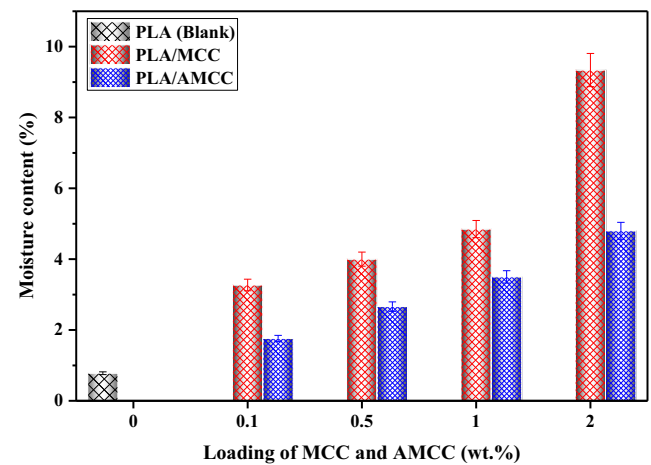


Fig. 5 Moisture absorption of PLA (Blank), PLA/MCC and PLA/AMCC for different loadings

Table 1 WVP of PLA (Blank), PLA/MCC and PLA/AMCC composite films

| Samples | WVP (g/m ² /day) | | | | |
|-------------|------------------------------|-------------|-------------|-------------|-------------|
| | Loading in PLA matrix (wt.%) | | | | |
| | 0 | 0.1 | 0.5 | 1 | 2 |
| PLA (Blank) | 35.2 ± 0.14 | – | – | – | – |
| PLA/MCC | – | 35.5 ± 0.26 | 35.8 ± 0.29 | 36.1 ± 0.14 | 36.5 ± 0.27 |
| PLA/AMCC | – | 33.8 ± 0.21 | 33.2 ± 0.16 | 32.5 ± 0.18 | 32.0 ± 0.22 |

Figure 2 shows the images of the untreated MCC and AMCC powders suspended in water/toluene solvent system. The MCC did not leave the water phase even after shaking well. In case of AMCC, it migrated completely in toluene phase and did not enter the aqueous phase even after shaking vigorously due to its hydrophobic character. Thus, the modification of the MCC with the acyl chain of olive oil has been successfully carried out [30, 32].

FTIR spectra of MCC and AMCC are shown in Fig. 3a. The obtained spectra of AMCC gave a clear confirmation of the occurrence of esterification by the appearance of a new peak at 1745 cm⁻¹ after the modification reaction which was attributed to the ester bond formation [30]. It can be clearly observed that the single absorptive band at 2900 cm⁻¹ in the MCC has changed to double absorptive bands at about 2854 cm⁻¹ and 2926 cm⁻¹ in the AMCC which could be related to the introduction of more methylene groups (C–H bonds) associated with acyl substitution [37–39]. The strong and broad band at 3342 cm⁻¹ is assigned to the stretching of hydroxyl groups [40, 41]. Also, the intensity of this peak was subdued for AMCC sample, confirming that the acyl group was successfully introduced on MCC.

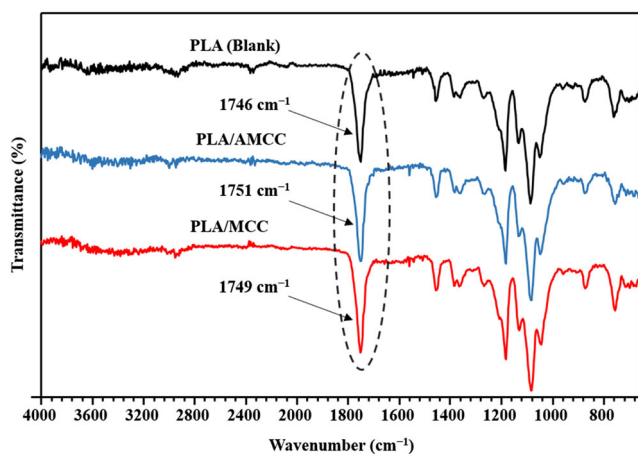
The effect on crystallinity after the modification was further examined using XRD analysis. The diffraction patterns of MCC and AMCC are illustrated in Fig. 3b. The MCC

exhibited the characteristic diffraction pattern of cellulose I, with the main diffraction angle 2θ at around 14.84°, 16.60°, 22.36° and 34.27° associated to the diffraction planes 101, 10 $\bar{1}$, 002, and 040, respectively. After the modification, the diffraction peaks have slightly shifted to the left side and showed a broadening in the intensities of the signals ascribed to the 101 and 002 planes and a decrease in the intensity of the related 040 diffraction planes. These changes were accompanied by an increase in the diffraction intensity at 2θ = 18°, which is normally assigned to the less ordered regions of cellulose chains [42].

The XRD results show that modification of MCC increased the amorphous regions in the AMCC. The crystallinity of unmodified MCC and AMCC were found to be 79.98% and 75.56% respectively indicating that the original crystalline structure of the MCC is only marginally affected. XRD results when studied together with FTIR, indicated that the substitution of the –OH group by acyl chain of olive oil, broke the inter- and intra-molecular hydrogen bonds of MCC and reduced its degree of crystallinity. Similar observations have been reported earlier [34, 42]. They also found the widening in diffraction peaks with an increase in a treatment time of different fatty acids applied on different cellulosic fibers.

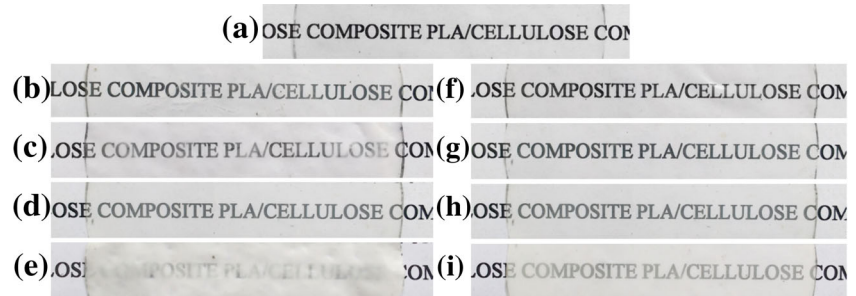
Thickness of PLA composite films

Figure 4 shows the thickness of PLA (blank) and PLA composite with different loading of MCC and AMCC. As a loading of reinforcement increases, the thickness of composite films also increased. However, the increase in thickness was

**Fig. 6** FTIR spectra of PLA (Blank), and composite films with 2 wt.% loading of MCC and AMCC**Table 2** FTIR peaks and bond details for PLA (Blank)

| Associated chemical group | Wavenumber (cm ⁻¹) |
|-------------------------------------|--------------------------------|
| C-O | 1180 |
| -C-H deformation | 1380 |
| -CH ₃ bending | 1452 |
| C=O stretching | 1747 |
| C-H (double) | 2983 |
| Stretching vibrations of –OH groups | Near 3500 |

Fig. 7 Photograph of PLA (Blank) (a), PLA/MCC with MCC loading of 0.1 (b), 0.5 (c), 1 (d) and 2 wt.% (e) PLA/AMCC with AMCC loading of 0.1 (f), 0.5 (g), 1 (h) and 2 wt.% (i)



only 22%. A similar result was reported for nanocomposite methylcellulose films also [43].

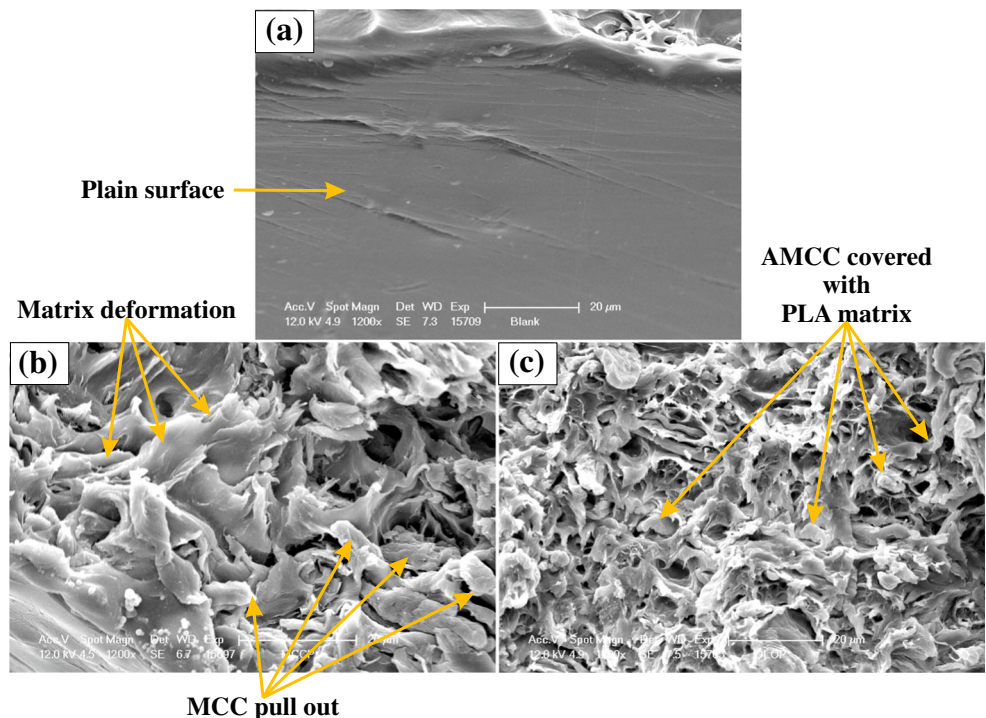
Moisture absorption of PLA composite films

Moisture absorption of the samples are shown in Fig. 5. It is precisely seen that moisture absorption of PLA/MCC composite film was always higher than the corresponding PLA/AMCC samples. The higher water absorption for the PLA/MCC samples was most likely due to the presence of hydrophilic MCC in the composite film. Also, the tendency of the PLA/AMCC composite film to absorb less water is attributed the hydrophobic character of the AMCC and stronger interfacial bonding with the matrix. Moreover, AMCC was homogeneously distributed throughout the matrix and shows less agglomeration whereas MCC formed small lumps in the composite film and hence less interaction with the PLA matrix [44].

WVP tests

WVP is one of the most properties in packaging films due to the important role of water in deteriorative reactions [45]. Table 1 shows the WVP values for all the three composite films. It is noted that the PLA/AMCC samples exhibited lower permeability values than the PLA (Blank) and PLA/MCC because of hydrophilic nature of MCC which influences the flow of water vapour property of composite films [34, 46, 47] This characteristic is essential for food packaging applications [34, 46]. The lower value of WVP of PLA/AMCC could be ascribed to different reasons like high crystalline structure (explained in the XRD section) and hydrophobic characteristics of AMCC in comparison to PLA matrix, making the tortuous path for water molecules in PLA matrix to pass through [34, 47]. AMCC dispersed well in the PLA matrix, and hence the flow of water vapours

Fig. 8 SEM images of PLA (Blank) (a), PLA/MCC (b) and PLA/AMCC (c) with 2 wt.% loading of MCC and AMCC respectively at 1200X



is more effectively block. However, in case of MCC, the dispersion was not good leading to agglomeration of particles in a matrix which increases crystallinity may provide channels or domains in the composite film that allows rapid permeation. Same observation was reported by *Paralikar et al.* [48] who examined the effect of cellulose nanocrystal on the barrier properties of cellulose nanocrystal/poly(vinyl alcohol) composite films.

FTIR analysis of PLA composite film

FTIR spectra of PLA (Blank), PLA/MCC and PLA/AMCC composite films are shown in Fig. 6. The important typical peaks of PLA (Blank) are mentioned in Table 2 [49]. The broad peak at 3400 cm^{-1} of PLA/MCC composite film indicated the presence of -OH group of MCC [41]. The intensity of this peak decreased in PLA/AMCC composite film due to the modification of MCC by olive oil, where hydroxyl groups were replaced by acyl group [30]. Furthermore, peak at 1747 cm^{-1} of PLA (Blank) corresponding to C=O stretching has shifted towards high wavenumber region in PLA/MCC and PLA/AMCC. The shift was more for PLA/AMCC. From this observation, it can be confirmed that hydrogen bonding between MCC and PLA matrix has taken place [49]. At the same time, intermolecular interaction through the C=O between the AMCC and PLA matrix has also happened [40].

The spectra of PLA/MCC and PLA/AMCC are almost similar. However, it was observed that intensity of wavenumber region 1747 cm^{-1} corresponding to C=O stretching which appears in PLA increased significantly in PLA/MCC followed by PLA/AMCC composite film. The increasing intensity of C=O stretching of PLA/MCC signifies the esterification reaction between -OH of MCC and terminal -COOH group of PLA [49]. Whereas in PLA/AMCC composite film, there is an intermolecular interaction between C=O of AMCC and PLA as well as unreacted -OH group of AMCC and terminal -COOH group of PLA [40, 49].

Morphological analysis of composite film

Figure 7 shows the photographs of PLA (Blank), PLA/MCC and PLA/AMCC composite films. Both the composite films maintained the transparent property of the PLA matrix. However, AMCC containing sample appeared more transparent than MCC composite film due to its better dispersion ability in the polymer matrix.

Figure 8 shows fractured surfaces of PLA (Blank), PLA/MCC and PLA/AMCC composite films. The smooth surface was seen for PLA (Blank) sample while the uneven fractured

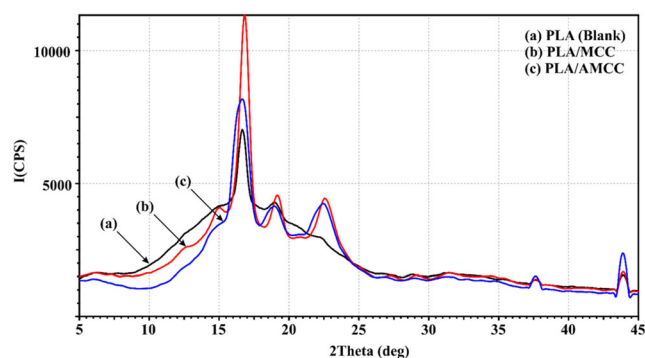


Fig. 9 XRD of PLA (Blank), and composite films with 2 wt.% loading of MCC and AMCC

surface was observed in case of composite films indicating major matrix deformation after the addition of MCC and AMCC [40, 50]. Similar micrographs were reported by *Mukherjee et al.* [1].

From Fig. 8b, the adhesion between PLA matrix and MCC was weaker as observed by the presence of several MCC pull-outs and the gaps between the MCC and PLA matrix [40, 49, 50]. SEM image of PLA/AMCC composite film indicated a uniform distribution of AMCC in PLA matrix (Fig. 8c). The capacity of acylation of MCC by olive oil to reduce filler-filler interactions through the reduction of surface energy resulted in better AMCC dispersion in PLA matrix. Furthermore, it was observed that PLA matrix covered AMCC with thin layer probably caused by the interaction between acyl group and PLA matrix [40, 50].

XRD analysis

The PLA (Blank), PLA/MCC and PLA/AMCC were analysed by X-ray diffraction to study the influence of MCC and

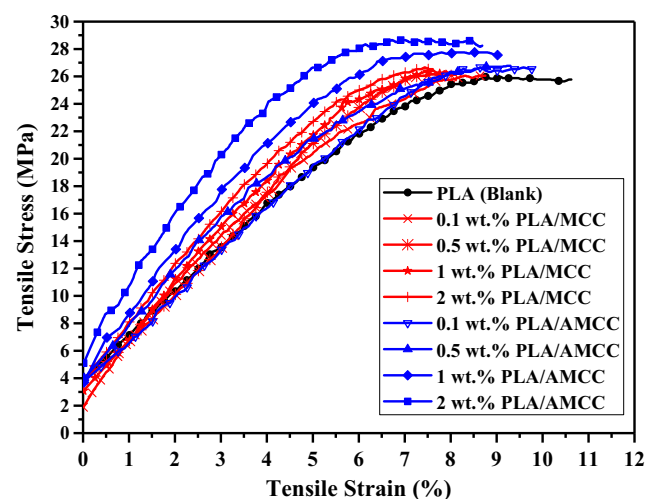


Fig. 10 Tensile stress-strain curves of PLA (Blank), and composite films with different loading of MCC and AMCC

AMCC on the crystallinity of PLA polymer. The diffractograms are presented in Fig. 9. Typical peaks of PLA were seen at $2\theta = 16.50^\circ, 19^\circ, 22.50^\circ$ and 43.90° , corresponding to different crystal structures [40].

Introduction of MCC and AMCC in PLA matrix increased the crystallinity of PLA, as shown by increased intensity and sharpness of the peaks. As the amount of MCC and AMCC increases, the crystallinity of corresponding composite sample also increases (not shown in Fig. 9). The crystallinity values of PLA (Blank), PLA/MCC and PLA/AMCC were 25%, 33% and 31.2% respectively. This value proves that MCC and AMCC accelerated crystallization of PLA. PLA/MCC has high crystallinity due to high crystallinity and self-aggregation of MCC in PLA matrix. The PLA polymer has both amorphous and crystalline phase arranged randomly. When AMCC is added in PLA matrix, uniform dispersion increased the crystallinity of the composite film [40]. This result is in line with the earlier results published by Lin et al. [51] where the crystallinity of the nanocrystal increased the intensity of peaks at 16.4° and 22.6° .

Mechanical properties of PLA composite film

Tensile stress versus tensile strain graph of PLA (Blank), PLA/MCC and PLA/AMCC composite films are presented in Fig. 10. PLA/MCC and PLA/AMCC composite films exhibited higher strength and stiffness as compared to PLA (Blank). Elongation-at-break of the composite films decreased as compared to that of PLA (Blank) which indicates that addition of MCC and AMCC in PLA matrix increased its brittleness.

Tensile modulus and elongation at break of PLA (Blank), PLA/MCC and PLA/AMCC composite films are shown in Fig. 11a, b respectively, while tensile strength is shown in Fig. 11c. Among all the three composite films, PLA/AMCC exhibited highest mechanical properties due to sufficient interfacial adhesion between AMCC and PLA matrix [49].

The tensile modulus and tensile strength of the PLA/MCC and PLA/AMCC composite increased gradually with an increase in the MCC and AMCC content respectively (Fig. 11a, c), whereas elongation at break decreases (Fig. 11b). In this case, the tensile strength of the 2 wt.%

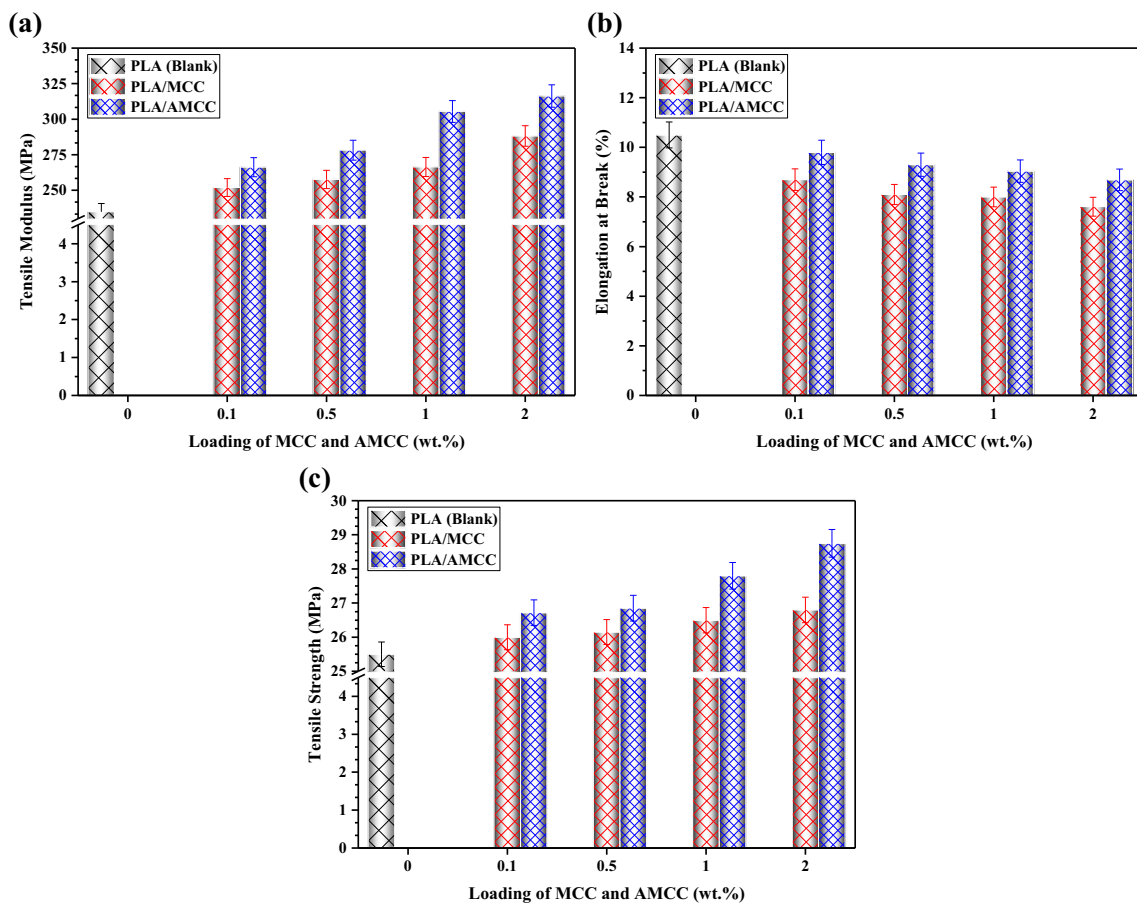


Fig. 11 Tensile properties of PLA (Blank), and composite films with different loading of MCC and AMCC: tensile modulus (a); elongation-at-break (b); tensile strength (c)

PLA/AMCC film reached a maximum value of 28.75 MPa, a 13% increase over the tensile strength of the PLA (Blank) film (25.5 MPa). Whereas in case of 2 wt.% PLA/MCC the tensile strength was found 26.8 MPa which is 4.12% higher than PLA (Blank). All the PLA/MCC and PLA/AMCC composites exhibited intensely increased tensile modulus values, and the composite with the highest loading level, 2 wt.% PLA/AMCC had the maximum tensile modulus value of 316.31 MPa, which was about 35% greater than that of the pure PLA film (234.91 MPa). The 2 wt.% PLA/MCC composite had tensile modulus value of 288.17 MPa, which is lower than 2 wt.% PLA/AMCC but greater than PLA (blank) film. Incorporation of MCC in PLA matrix decreased the elongation of the composite film in comparison to that of PLA (Blank) and PLA/AMCC composite film due to agglomeration and uneven distribution of MCC (Fig. 11b). Also, the addition of AMCC in PLA matrix decreased elongation at break.

The higher value of PLA/AMCC was due to the better interfacial adhesion between AMCC filler and PLA matrix (discussed in FTIR and SEM analysis). Similar results were reported for the composite film reinforced with acylated, silylated and chemical grafted cellulose materials

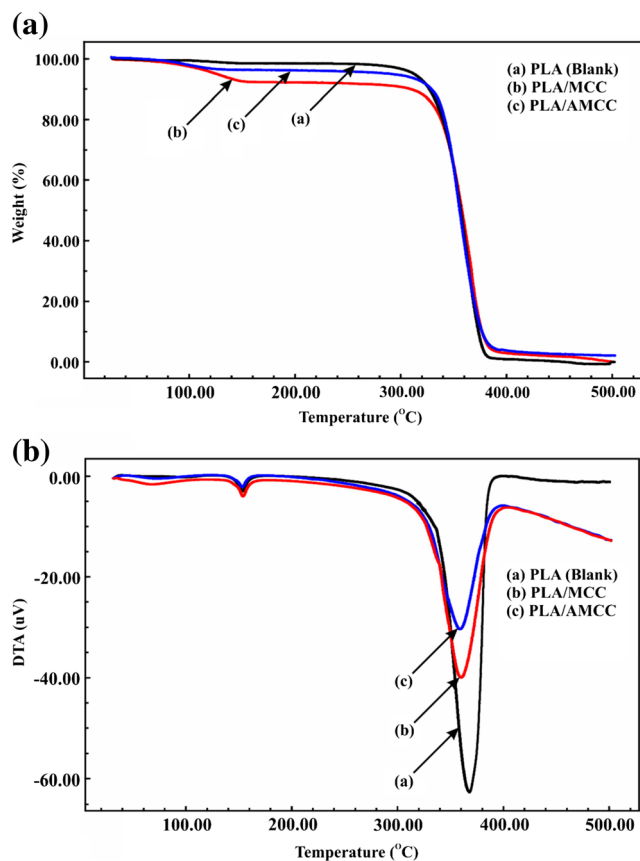


Fig. 12 TGA (a), DTA (b) curves for PLA (Blank) and composite films with 2 wt.% loading of MCC and AMCC

Table 3 Melting temperature (T_m), initial decomposition temperature (T_{di}), and maximum decomposition temperature (T_{dmax}) of PLA (Blank), PLA composite films (2 wt.% loading each of MCC and AMCC) from TGA and DTG curve

| Sample | TGA | | |
|-------------|------------|---------------|-----------------|
| | T_m (°C) | T_{di} (°C) | T_{dmax} (°C) |
| PLA (Blank) | 153.51 | 338.97 | 372.45 |
| PLA/MCC | 153.19 | 334.22 | 374.39 |
| PLA/AMCC | 153.74 | 339.49 | 378.15 |

[8]. However, *Almasi et al.* [34] and *Lin et al.* [52] observed increased in modulus, strength and decreased in elongation at break of cellulose nanofiber chemically modified by oleic acid and acetic anhydride respectively, as compared with PLA film. *Yu et al.* [53] reported the addition of silylated ramie fibres in PLA matrix showed higher elongation at break in comparison to neat PLA. Thus, we can propose that reinforcing the effect of filler is dependent on its modification method and dispersibility in the polymer matrix [34].

Thermal properties

TGA and DTA curves of PLA (Blank), PLA/MCC and PLA/AMCC composite film materials are shown in Fig. 12.

For PLA (Blank) the weight loss took place only in a single step in the range between 338 °C to 373 °C due to the depolymerization of PLA (Fig. 12b). From Fig. 12a, the thermal decomposition process of PLA/MCC and PLA/AMCC composite films exhibit two steps of weight loss. Their thermal stability depends on hydrophilic and hydrophobic properties of reinforcement in PLA matrix. The first weight loss step in the range of 80 °C to 130 °C was due to evaporation of moisture absorbed by

Table 4 UV transmittance and UV-protection factor values of PLA (Blank) and PLA composite film with different loading of MCC and AMCC

| Sample | Loading of MCC and AMCC (wt.%) | UVA | UVB | UPF |
|-------------|--------------------------------|---------------|---------------|---------------|
| | | 315 nm~400 nm | 290 nm~315 nm | 290 nm~400 nm |
| PLA (Blank) | | 86.34 | 76.16 | 1.24 |
| PLA/MCC | 0.1 | 48.42 | 43.62 | 2.21 |
| | 0.5 | 49.28 | 41.19 | 2.30 |
| | 1 | 46.90 | 30.39 | 2.83 |
| | 2 | 21.75 | 6.43 | 11.34 |
| PLA/AMCC | 0.1 | 56.39 | 47.67 | 1.98 |
| | 0.5 | 46.66 | 40.11 | 2.37 |
| | 1 | 34.20 | 16.24 | 4.99 |
| | 2 | 0.69 | 0.15 | 470.80 |

reinforcement materials. However, compared to PLA/MCC, PLA/AMCC have a lower moisture evaporation. Because of low moisture absorbed by AMCC dispersed in PLA matrix [54]. The second mass loss was in the range of approximately 334 °C to 378 °C attributed to the decomposition of cellulose in the composite film and depolymerization of PLA [55].

Thermal stability of the composite films (Table 3) was observed to be slightly better than the PLA (Blank). Between two composite films, PLA/AMCC was more stable due to the excellent compatibility between PLA and AMCC. Similar observations were made in the previous report by Wang et al. [56], where silane treated sisal fibres showed significant thermal stability. Also, Martins et al. & Trovatti et al. reported the same behaviour for bacterial cellulose composite films with thermoplastic starch [57] and acrylic thermoplastic resins respectively.

UV-protection of PLA and PLA composite films

For packaging material, UV light barrier property is a most important factor regarding the protection of light-sensitive products during storage. When plastic materials exposed to

UV radiation (200 to 400 nm), it undergoes photochemical degradation. PLA is commonly used as a packaging material, but its weak UV barrier property limits its applications [58]. The UV transmittance (UVA and UVB) and UPF values of PLA (Blank) and PLA composite films for different wt.% loading of MCC and AMCC are reported in Table 4. Figure 13 shows the UV transmittance spectra of PLA and PLA composite films.

It can be seen from the Table 4 that PLA (Blank) films allow passage of ~86% and ~76% of radiation in the UV-A and UV-B regions, respectively. This value decreased with increasing loading of MCC and AMCC in PLA matrix. According to the UV protection factor (UPF, AS/NZS 4399), the samples can be evaluated as providing good 15 < UPF < 24, very good in 24 < UPF < 39, and excellent protection in UPF > 39. With loading of 1 wt.% MCC and AMCC composite films show UPF value less than 15. The UPF factors of PLA composite film with 2 wt.% loading of AMCC are over 100, which means excellent UV protection is mainly attributed to the absorption of UV radiation by AMCC particles and uniform distribution of AMCC throughout PLA matrix. In case of PLA composite film with 2 wt.% loading of MCC

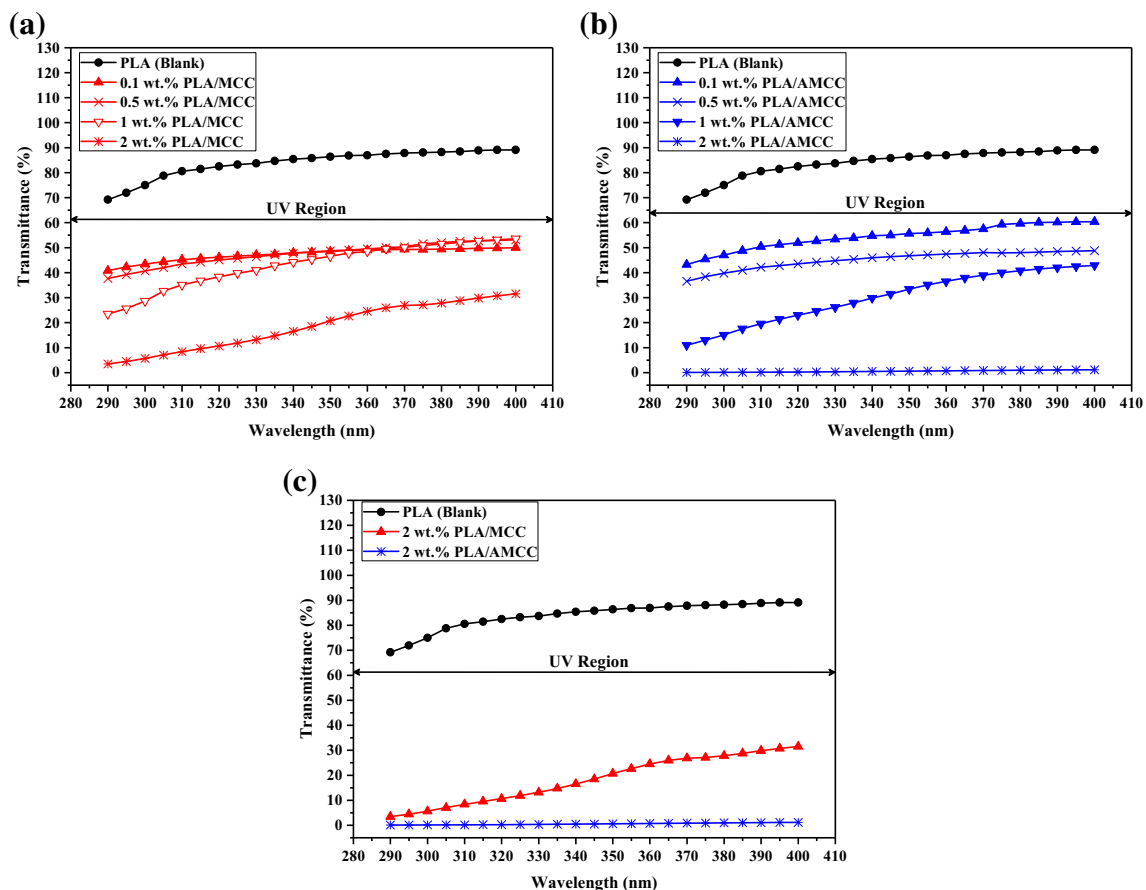


Fig. 13 UV transmittance of PLA (Blank) and PLA composite films with different loading of MCC (a) and AMCC (b); 2 wt.% loading of MCC and AMCC (c)

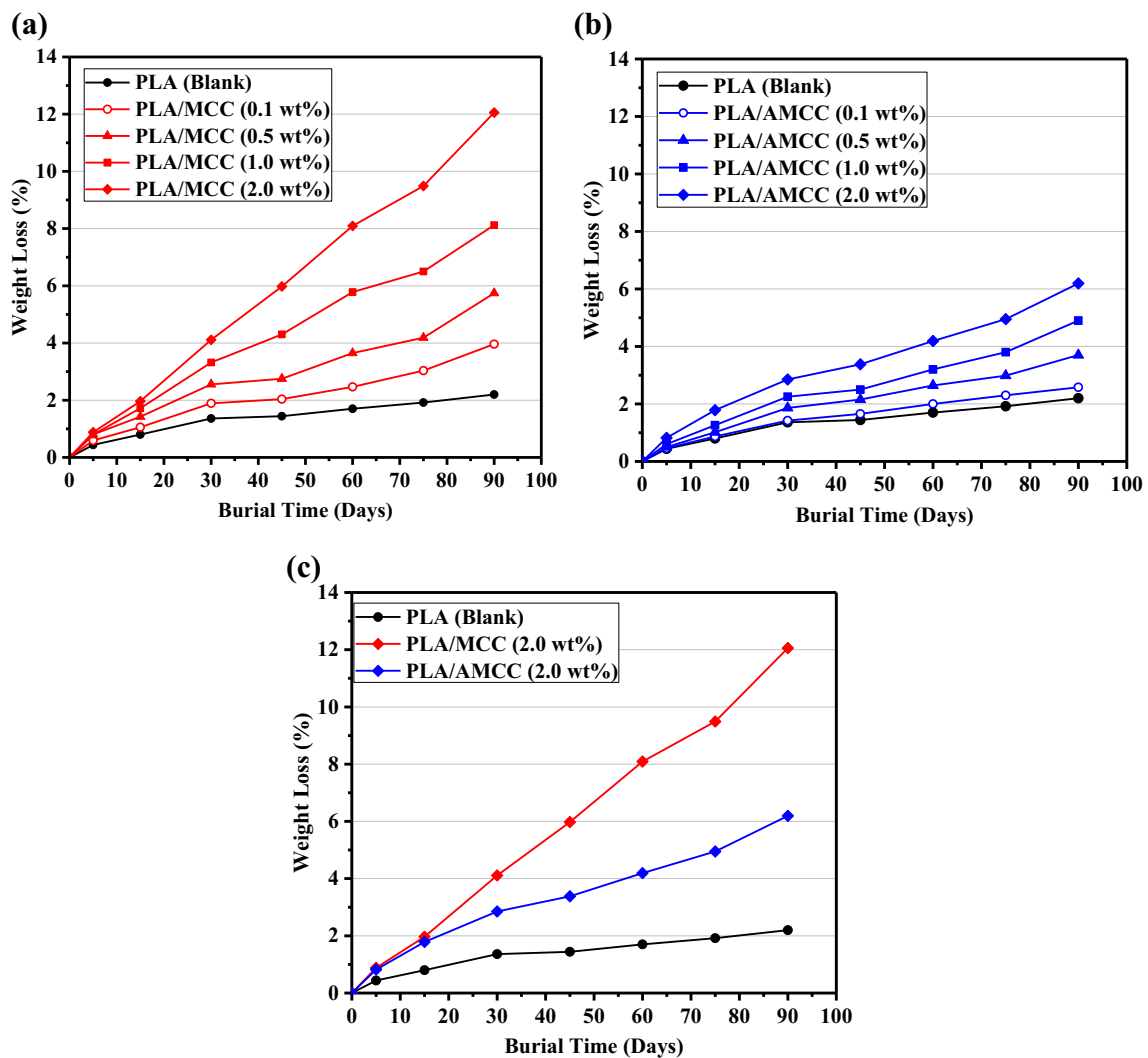


Fig. 14 Effect of MCC (a), AMCC (b) loading on weight loss of PLA composite film, and % weight loss of PLA (Blank) and PLA composite film with 2 wt.% loading of MCC and AMCC (c)

show UPF value of 11.34 owing to the aggregation of MCC particles which create space for passing radiation.

Biodegradability of PLA composite films

Composting is the most preferred disposal route to determine biodegradability. Figure 14 gives the % weight loss of PLA/MCC and PLA/AMCC composite films with different loadings of MCC and AMCC respectively along with its comparison with PLA (Blank). From Fig. 14a, b, the % weight loss of composite films was linear with time. The weight loss of PLA (Blank) was found to be 2.2%, whereas weight loss of PLA/MCC and PLA/AMCC with the loading of 2 wt.% was 12.05% and 6.29% respectively (Fig. 14c). The weight loss of PLA/MCC was higher compared with a weight loss of PLA/AMCC due to poor adhesion of hydrophilic MCC and PLA matrix leading to a faster rate of degradation [59]. At the same time,

hydrophobic nature of AMCC dispersed in PLA/AMCC composite film had low moisture absorption ability from soil leading to a reduction in the rate of the degradation but still better than neat PLA [33].

Conclusion

The hydrophobic modification of MCC by olive oil was successfully performed by replacing OH groups with acyl groups on the surface of MCC, AMCC migrated in toluene in water/toluene system after modification with reduced crystallinity by 3.85%. The results of the study proved that surface treatment of MCC improved the compatibility with PLA matrix. PLA/AMCC composite film showed lower moisture absorption than PLA/MCC. FTIR analysis confirmed the formation of the various chemical as well as physical bonding associated with MCC, AMCC and PLA

components. Water vapour permeability of PLA/AMCC was decreased by increasing the reinforcement loading. The crystallinity of PLA/MCC (33%) was higher than PLA/AMCC (31%) followed by neat PLA film (25%). The tensile strength of the 2 wt.% PLA/AMCC composite was enhanced by as much as 13% and the tensile modulus by 1.4-fold than those of the PLA (Blank). This was mainly attributed to the enhanced interfacial adhesion with PLA matrix as observed by the SEM analysis. Thermal stability of composite films was improved after addition of MCC and AMCC in the matrix. The PLA composite films with 2 wt.% loading of AMCC have desirable (470 UPF value) UV light barrier properties. Biodegradability of both the composite film was higher than PLA (Blank) sample. The resultant composite film can find application in food packaging, plastic cups, transparent film, decomposable packaging material, carry bags etc.

Acknowledgements One of the authors Vikrant G. Gorade is indebted to World Bank-funded TEQIP-II - CoE in Process Intensification, for the scholarship support during the Ph.D. course. The authors would like to thank the DST-FIST for providing testing facilities.

Author contributions The manuscript was written through contributions of all authors. All authors have given approval to the final version of the manuscript. ‡Vikrant G. Gorade contributed equally to this work.

Compliance with ethical standards

Conflict of interest The authors declare no competing financial interest.

References

- Mukherjee T, Sani M, Kao N et al (2013) Improved dispersion of cellulose microcrystals in polylactic acid (PLA) based composites applying surface acetylation. *Chem Eng Sci* 101:655–662. <https://doi.org/10.1016/j.ces.2013.07.032>
- Guo W, Bao F, Wang Z (2013) Biodegradability of wood fiber/poly(lactic acid) composites. *J Compos Mater* 47:3573–3580. <https://doi.org/10.1177/0021998312467387>
- Tunç S, Duman O (2011) Preparation of active antimicrobial methyl cellulose/carvacrol/montmorillonite nanocomposite films and investigation of carvacrol release. *LWT-Food Sci Technol* 44:465–472. <https://doi.org/10.1016/j.lwt.2010.08.018>
- Kumar S, Koh J (2014) Physiochemical and optical properties of chitosan based graphene oxide bionanocomposite. *Int J Biol Macromol* 70:559–564. <https://doi.org/10.1016/j.ijbiomac.2014.07.019>
- Çetin NS, Özmen Çetin N, Harper DP (2015) Vinyl acetate-modified microcrystalline cellulose-reinforced HDPE composites prepared by twin-screw extrusion. *Turk J Agric For* 39:39–47. <https://doi.org/10.3906/tar-1402-115>
- Dubief D, Samain E, Dufresne A (1999) Polysaccharide microcrystals reinforced amorphous poly(β -hydroxyoctanoate) nanocomposite materials. *Macromolecules* 32:5765–5771. <https://doi.org/10.1021/ma990274a>
- Ten E, Turtle J, Bahr D et al (2010) Thermal and mechanical properties of poly(3-hydroxybutyrate-co-3-hydroxyvalerate)/cellulose nanowhiskers composites. *Polymer (Guildf)* 51:2652–2660. <https://doi.org/10.1016/j.polymer.2010.04.007>
- Habibi Y, Dufresne A (2008) Highly filled bionanocomposites from functionalized polysaccharide nanocrystals. *Biomacromolecules* 9:1974–1980. <https://doi.org/10.1021/bm8001717>
- Ruiz MM, Cavaillé JY, Dufresne A et al (2000) Processing and characterization of new thermoset nanocomposites based on cellulose whiskers. *Compos Interfaces* 7:117–131. <https://doi.org/10.1163/156855400300184271>
- Garcia de Rodriguez NL, Thielemans W, Dufresne A (2006) Sisal cellulose whiskers reinforced polyvinyl acetate nanocomposites. *Cellulose* 13:261–270. <https://doi.org/10.1007/s10570-005-9039-7>
- Chazeau L, Cavaillé JY, Terech P (1999) Mechanical behaviour above T(g) of a plasticised PVC reinforced with cellulose whiskers; a SANS structural study. *Polymer (Guildf)* 40:5333–5344. [https://doi.org/10.1016/S0032-3861\(98\)00748-4](https://doi.org/10.1016/S0032-3861(98)00748-4)
- Chazeau L, Paillet M, Cavaillé JY (1999) Plasticized PVC reinforced with cellulose whiskers. I. Linear viscoelastic behavior analyzed through the quasi-point defect theory. *J Polym Sci Part B Polym Phys* 37:2151–2164. [https://doi.org/10.1002/\(SICI\)1099-0488\(19990815\)37:16<2151::AID-POLB17>3.0.CO;2-V](https://doi.org/10.1002/(SICI)1099-0488(19990815)37:16<2151::AID-POLB17>3.0.CO;2-V)
- Liu D, Zhong T, Chang PR et al (2010) Starch composites reinforced by bamboo cellulosic crystals. *Bioresour Technol* 101:2529–2536. <https://doi.org/10.1016/j.biortech.2009.11.058>
- Marcovich NE, Auad ML, Bellesi NE et al (2006) Cellulose micro/nanocrystals reinforced polyurethane. *J Mater Res* 21:870–881. <https://doi.org/10.1557/jmr.2006.0105>
- Bondeson D, Oksman K (2007) Polylactic acid/cellulose whisker nanocomposites modified by polyvinyl alcohol. *Compos A Appl Sci Manuf* 38:2486–2492. <https://doi.org/10.1016/j.compositesa.2007.08.001>
- Petersson L, Kvien I, Oksman K (2007) Structure and thermal properties of poly(lactic acid)/cellulose whiskers nanocomposite materials. *Compos Sci Technol* 67:2535–2544. <https://doi.org/10.1016/j.compscitech.2006.12.012>
- Oksman K, Mathew AP, Bondeson D, Kvien I (2006) Manufacturing process of cellulose whiskers/poly(lactic acid) nanocomposites. *Compos Sci Technol* 66:2776–2784. <https://doi.org/10.1016/j.compscitech.2006.03.002>
- Kale G, Auras R, Singh SP (2006) Degradation of commercial biodegradable packages under real composting and ambient exposure conditions. *J Polym Environ* 14:317–334. <https://doi.org/10.1007/s10924-006-0015-6>
- Mohammed L, Ansari MNM, Pua G et al (2015) A review on natural fiber reinforced polymer composite and its applications. *Int J Polym Sci* 2015:1–15. <https://doi.org/10.1155/2015/243947>
- Peydecastaing J, Vaca-Garcia C, Borredon E (2011) Bi-acylation of cellulose: determining the relative reactivities of the acetyl and fatty-acyl moieties. *Cellulose* 18:1015–1021. <https://doi.org/10.1007/s10570-011-9528-9>
- Lu J, Askeland P, Drzal LT (2008) Surface modification of microfibrillated cellulose for epoxy composite applications. *Polymer (Guildf)* 49:1285–1296. <https://doi.org/10.1016/j.polymer.2008.01.028>
- Paul A, Joseph K, Thomas S (1997) Effect of surface treatments on the electrical properties of low-density polyethylene composites reinforced with short sisal fibers. *Compos Sci Technol* 57:67–79. [https://doi.org/10.1016/S0266-3538\(96\)00109-1](https://doi.org/10.1016/S0266-3538(96)00109-1)
- Kabir MM, Wang H, Lau KT, Cardona F (2012) Chemical treatments on plant-based natural fibre reinforced polymer composites: an overview. *Compos Part B Eng* 43:2883–2892. <https://doi.org/10.1016/j.compositesb.2012.04.053>
- Lindqvist J, Malmström E (2006) Surface modification of natural substrates by atom transfer radical polymerization. *J Appl Polym Sci* 100:4155–4162. <https://doi.org/10.1002/app.23457>

25. Kim DY, Nishiyama Y, Kuga S (2002) Surface acetylation of bacterial cellulose. *Cellulose* 9:361–367. <https://doi.org/10.1023/A:1021140726936>
26. Ismail H, Rusli A, Rashid AA (2005) Maleated natural rubber as a coupling agent for paper sludge filled natural rubber composites. *Polym Test* 24:856–862. <https://doi.org/10.1016/j.polymertesting.2005.06.011>
27. Yuan H, Nishiyama Y, Wada M, Kuga S (2006) Surface acylation of cellulose whiskers by drying aqueous emulsion. *Biomacromolecules* 7:696–700. <https://doi.org/10.1021/bm050828j>
28. Hidayat A, Tachibana S (2012) Characterization of polylactic acid (PLA)/kenaf composite degradation by immobilized mycelia of *Pleurotus ostreatus*. *Int Biodeterior Biodegrad* 71:50–54. <https://doi.org/10.1016/j.ibiod.2012.02.007>
29. Hao Y, Peng J, Li J et al (2009) An ionic liquid as reaction media for radiation-induced grafting of thermosensitive poly (N-isopropylacrylamide) onto microcrystalline cellulose. *Carbohydr Polym* 77:779–784. <https://doi.org/10.1016/j.carbpol.2009.02.025>
30. Dankovich TA, Hsieh YL (2007) Surface modification of cellulose with plant triglycerides for hydrophobicity. *Cellulose* 14:469–480. <https://doi.org/10.1007/s10570-007-9132-1>
31. Phillips DL, Liu H, Pan D, Corke H (1999) General application of Raman spectroscopy for the determination of level of acetylation in modified starches. *Cereal Chem* 76:439–443. <https://doi.org/10.1094/CCHEM.1999.76.3.439>
32. Namazi H, Dadkhah A (2010) Convenient method for preparation of hydrophobically modified starch nanocrystals with using fatty acids. *Carbohydr Polym* 79:731–737. <https://doi.org/10.1016/j.carbpol.2009.09.033>
33. Gunti R, Ratna Prasad AV, Gupta AVSSKS (2016) Mechanical and degradation properties of natural fiber reinforced PLA composites: jute, sisal, and elephant grass. *Polym Compos*. <https://doi.org/10.1002/pc.24041>
34. Almasi H, Ghanbarzadeh B, Dehghannya J et al (2015) Novel nanocomposites based on fatty acid modified cellulose nanofibers/poly(lactic acid): morphological and physical properties. *Food Packag Shelf Life* 5:21–31. <https://doi.org/10.1016/j.fpsl.2015.04.003>
35. American Society for Testing and Materials (2010) ASTM E96/E96M-10 standard test methods for water vapor transmission. *Annu B ASTM Stand* 4:1–12. https://doi.org/10.1520/E0096_E0096M-10
36. Keshk SMAS, Yousef E, Omran A (2015) Preparation and characterization of starch/cellulose composite. *Indian J Fibre Text Res* 40: 190–194
37. Vlachos N, Skopelitis Y, Psaroudaki M et al (2006) Applications of Fourier transform-infrared spectroscopy to edible oils. *Anal Chim Acta* 573–574:459–465. <https://doi.org/10.1016/j.aca.2006.05.034>
38. Liang P, Chen C, Zhao S et al (2013) Application of fourier transform infrared spectroscopy for the oxidation and peroxide value evaluation in virgin walnut oil. *J Spectrosc*:1:1–1:5. <https://doi.org/10.1155/2013/138728>
39. Kale RD, Gorade VG, Bhor S (2017) Preparation of self-reinforced cellulose composite using microcrystalline cellulose. *Indian J Sci Res* 16:3–6
40. Mukherjee T, Tobin MJ, Puskar L et al (2017) Chemically imaging the interaction of acetylated nanocrystalline cellulose (NCC) with a polylactic acid (PLA) polymer matrix. *Cellulose* 24:1717–1729. <https://doi.org/10.1007/s10570-017-1217-x>
41. Kale RD, Bansal PS, Gorade VG (2017) Extraction of microcrystalline cellulose from cotton sliver and its comparison with commercial microcrystalline cellulose. *J Polym Environ* 26:355–364. <https://doi.org/10.1007/s10924-017-0936-2>
42. Freire CSR, Silvestre AJD, Neto CP et al (2006) Controlled heterogeneous modification of cellulose fibers with fatty acids: effect of reaction conditions on the extent of esterification and fiber properties. *J Appl Polym Sci* 100:1093–1102. <https://doi.org/10.1002/app.23454>
43. Tunç S, Duman O (2010) Preparation and characterization of biodegradable methyl cellulose/montmorillonite nanocomposite films. *Appl Clay Sci* 48:414–424. <https://doi.org/10.1016/j.clay.2010.01.016>
44. Kargarzadeh H, Sheltami RM, Ahmad I et al (2015) Cellulose nanocrystal: a promising toughening agent for unsaturated polyester nanocomposite. *Polym (United Kingdom)* 56:346–357. <https://doi.org/10.1016/j.polymer.2014.11.054>
45. Tunç S, Duman O, Polat TG (2016) Effects of montmorillonite on properties of methyl cellulose/carvacrol based active antimicrobial nanocomposites. *Carbohydr Polym* 150:259–268. <https://doi.org/10.1016/j.carbpol.2016.05.019>
46. Fortunati E, Peltzer M, Armentano I et al (2012) Effects of modified cellulose nanocrystals on the barrier and migration properties of PLA nano-biocomposites. *Carbohydr Polym* 90:948–956. <https://doi.org/10.1016/j.carbpol.2012.06.025>
47. Abdulkhali A, Hosseinzadeh J, Ashori A et al (2014) Preparation and characterization of modified cellulose nanofibers reinforced polylactic acid nanocomposite. *Polym Test* 35:73–79. <https://doi.org/10.1016/j.polymertesting.2014.03.002>
48. Paralikar SA, Simonsen J, Lombardi J (2008) Poly(vinyl alcohol)/cellulose nanocrystal barrier membranes. *J Membr Sci* 320:248–258. <https://doi.org/10.1016/j.memsci.2008.04.009>
49. Zafar MT, Maiti SN, Ghosh AK (2016) Effect of surface treatments of jute fibers on the microstructural and mechanical responses of poly(lactic acid)/jute fiber biocomposites. *RSC Adv* 6:73373–73382. <https://doi.org/10.1039/C6RA17894D>
50. Frone AN, Berlioz S, Chailan JF et al (2011) Cellulose fiber-reinforced polylactic acid. *Polym Compos* 32:976–985. <https://doi.org/10.1002/pc.21116>
51. Lin N, Chen G, Huang J et al (2009) Effects of polymer-grafted natural nanocrystals on the structure and mechanical properties of poly(lactic acid): a case of cellulose whisker-graft-polycaprolactone. *J Appl Polym Sci* 113:3417–3425. <https://doi.org/10.1002/app.30308>
52. Lin N, Huang J, Chang PR et al (2011) Surface acetylation of cellulose nanocrystal and its reinforcing function in poly(lactic acid). *Carbohydr Polym* 83:1834–1842. <https://doi.org/10.1016/j.carbpol.2010.10.047>
53. Yu T, Ren J, Li S et al (2010) Effect of fiber surface-treatments on the properties of poly(lactic acid)/ramie composites. *Compos A Appl Sci Manuf* 41:499–505. <https://doi.org/10.1016/j.compositesa.2009.12.006>
54. Suchaiya V, Aht-Ong D (2014) Microwave-assisted modification of cellulose as a compatibilizer for PLA and MCC biocomposite film: effects of side chain length and content on mechanical and thermal properties. *Polym Polym Compos* 22:613–624
55. Tee YB, Talib RA, Abdan K et al (2013) Thermally grafting aminosilane onto kenaf-derived cellulose and its influence on the thermal properties of poly(lactic acid) composites. *Bioresources* 8: 4468–4483. <https://doi.org/10.15376/biores.8.3.4468-4483>
56. Wang Y, Tong B, Hou S et al (2011) Transcrystallization behavior at the poly(lactic acid)/sisal fibre biocomposite interface. *Compos A Appl Sci Manuf* 42:66–74. <https://doi.org/10.1016/j.compositesa.2010.10.006>
57. Martins IMG, Magina SP, Oliveira L et al (2009) New biocomposites based on thermoplastic starch and bacterial cellulose. *Compos Sci Technol* 69:2163–2168. <https://doi.org/10.1016/j.compscitech.2009.05.012>
58. Auras R, Harte B, Selke S (2004) An overview of polylactides as packaging materials. *Macromol Biosci* 4:835–864. <https://doi.org/10.1002/mabi.200400043>
59. Goriparthi BK, Suman KNS, Nalluri MR (2012) Processing and characterization of jute fiber reinforced hybrid biocomposites based on polylactide/polycaprolactone blends. *Polym Compos* 33:237–244. <https://doi.org/10.1002/pc.22145>